

The continuum elastic and atomistic viewpoints on the formation volume and strain energy of a point defect

K. Garikipati*, M. Falk†, M. Bouville‡, B. Puchala§, H. Narayanan ¶
University of Michigan, Ann Arbor, Michigan 48109, USA

October 2, 2018

Abstract

We discuss the roles of continuum linear elasticity and atomistic calculations in determining the formation volume and the strain energy of formation of a point defect in a crystal. Our considerations bear special relevance to defect formation under stress. The elasticity treatment is based on the Green's function solution for a center of contraction or expansion in an anisotropic solid. It makes possible the precise definition of a formation volume tensor and leads to an extension of Eshelby's result for the work done by an external stress during the transformation of a continuum inclusion (*Proc. Roy. Soc. Lond. Ser. A*, **241**(1226), 376, 1957). Parameters necessary for a complete continuum calculation of elastic fields around a point defect are obtained by comparing with an atomistic solution in the far field. However, an elasticity result makes it possible to test the validity of the formation volume that is obtained via atomistic calculations under various boundary conditions. It also yields the correction term for formation volume calculated under these boundary conditions. Using two types of boundary conditions commonly employed in atomistic calculations, a comparison is also made of the strain energies of formation predicted by continuum elasticity and atomistic calculations. The limitations of the continuum linear elastic treatment are revealed by comparing with atomistic calculations of the formation volume and strain energies of small crystals enclosing point defects.

*Assistant professor, Dept. of Mechanical Engineering, and Program in Applied Physics.
Corresponding author. krishna@umich.edu

†Assistant professor, Dept. of Materials Science and Engineering, and Program in Applied Physics.

‡Formerly, graduate research assistant, Dept. of Materials Science and Engineering. Now a post-doctoral fellow at Institute of Materials Research and Engineering, Singapore.

§Graduate research assistant, Dept. of Materials Science and Engineering.

¶Graduate research assistant, Dept. of Mechanical Engineering.

1 Introduction: Free energy of point defect formation under external stress

When a point defect forms in a crystal there are two main contributions to the Gibbs free energy of formation, $\mathcal{G}^f = (\mathcal{U}^f - T\mathcal{S}^f) - \mathcal{W}^{\text{ex}}$. The first comes from the internal energy of formation, \mathcal{U}^f , and the usually negligible entropic term $-T\mathcal{S}^f$, where T is the temperature and \mathcal{S}^f is the change in entropy. The second contribution arises due to the work done by the external stress, and can be formally written as $-\mathcal{W}^{\text{ex}} = -\boldsymbol{\sigma}^{\text{ex}} : \mathbf{V}^f$, where $\boldsymbol{\sigma}^{\text{ex}}$ is the external stress and \mathbf{V}^f is the “formation volume tensor”. The latter quantity is commonly used in the materials physics literature (see Aziz, 1997; Zhao et al., 1999a,b; Daw et al., 2001) and can be formally defined as $\mathbf{V}^f \equiv -\partial\mathcal{G}^f/\partial\boldsymbol{\sigma}^{\text{ex}}$. A related quantity, the migration volume tensor, $\mathbf{V}^m \equiv -\partial\mathcal{G}^m/\partial\boldsymbol{\sigma}^{\text{ex}}$, is associated with the free energy difference the ground state and the transition state that the system traverses when the defect hops between lattice sites. These quantities are of fundamental interest in materials physics. They influence the kinetics of transport through the diffusivity, $D = D_0 \exp[-(\mathcal{G}^f + \mathcal{G}^m)/k_B T]$, where k_B is the Boltzmann constant.¹ The thermodynamics of transport is influenced through the chemical potential, $\mu = \mu_0 - \boldsymbol{\sigma}^{\text{ex}} : (\mathbf{V}^f + \mathbf{V}^m)$, where μ_0 is the potential without stress effects.

It is natural to attempt a continuum treatment of point defects since their interaction with stress—a continuum quantity—is of central interest in this paper. Point defects are modelled as centers of contraction or expansion within continuum linear elasticity. While the idea of a formation volume tensor, introduced above in association with a point defect, is not standard in continuum mechanics, we place this notion on firm footing in Section 3. Additionally, the introduction of a formation volume that is energy-conjugate to the stress does have an analogue in linear elasticity: In a series of seminal papers on elastic inclusions Eshelby considered “cutting and welding” operations to describe the transformation of an inclusion within a solid that is itself under external stress (see, for instance, Eshelby, 1957, 1961). He was able to show that the work done is $\int \boldsymbol{\sigma}^{\text{ex}} : \boldsymbol{\varepsilon}^r dV$, where $\boldsymbol{\varepsilon}^r$ is the transformation strain due to relaxation, and the integral is over the inclusion. We also demonstrate in Section 3 that an extension of Eshelby’s result to point defects can be obtained in a rigorous manner, leading to the form $-\mathcal{W}^{\text{ex}} = -\boldsymbol{\sigma}^{\text{ex}} : \mathbf{V}^f$ introduced above.

The other goal of this communication is to discuss practical aspects surrounding the evaluation of \mathbf{V}^f and \mathcal{U}^f . On modelling a point defect as a center of contraction or expansion one can obtain a deformation field that clearly must bear some relation to \mathbf{V}^f and \mathcal{U}^f . Whatever these relations, \mathbf{V}^f and \mathcal{U}^f cannot be calculated unless the strength of the center of contraction or expansion, represented by a force dipole tensor, is specified in the elasticity problem. Indeed, in linear elasticity, all elastic fields scale with the dipole tensor. This quantity

¹Formation plays a role in self-diffusion of point defects, and in inter-diffusion, since both phenomena require the formation of a point defect that subsequently migrates. In doing so it may enable the migration of a substitutional atom (inter-diffusion).

must be obtained from some form of atomistic calculation, as is done in Section 3. However, the linearity of the theory enables us to show in Sections 3 and 4 that even without quantifying the dipole tensor, rather simple elasticity calculations reveal the influence of boundary conditions that are used in the atomistic simulations. A straightforward scaling with the correct dipole tensor then leads to the actual fields in elasticity. These calculations are carried out for the isotropic vacancy in silicon in this preliminary communication. The results are summarized and placed in the proper context in Section 5.

2 The continuum elastic model of a point defect

In continuum elasticity a point defect is modelled as an arrangement of point forces in a center of contraction or expansion. An associated dipole tensor is defined as²

$$\mathbf{D} = \sum_{i=1}^3 \mathbf{F}_i \otimes 2\mathbf{d}_i. \quad (1)$$

In the dipole illustrated in Figure 1 the forces are in equilibrium. Moments are also in equilibrium provided that \mathbf{D} is symmetric, which will be assumed here. In this case \mathbf{D} can be written with respect to an orthonormal set of basis vectors $\{\mathbf{e}_1, \mathbf{e}_2, \mathbf{e}_3\}$ that coincide with its own eigen vectors. In terms of this basis, \mathbf{D} is therefore diagonal. Furthermore, if the magnitudes of the point forces are equal: $|\mathbf{F}_1|, |\mathbf{F}_2|, |\mathbf{F}_3| = F$, and the magnitudes of the position vectors are also equal: $|\mathbf{d}_1|, |\mathbf{d}_2|, |\mathbf{d}_3| = d$, then \mathbf{D} is isotropic and can be written as

$$\mathbf{D} = D\mathbf{1}, \quad \text{where } D = \pm 2Fd, \quad (2)$$

and $\mathbf{1}$ is the second-order isotropic tensor. The positive sign in (2) holds for centers of contraction and the negative sign is for centers of expansion as is easily verified. The isotropy of \mathbf{D} , and $D > 0$ have been assumed for all numerical calculations in the paper. These choices correspond to an isotropic vacancy—one in which the magnitudes of displacements of the nearest-neighbor atoms are equal, or a substitutional defect with smaller atomic volume than the host atoms. If $D < 0$, it is an isotropic interstitial or an isotropic substitutional defect³ with larger atomic volume than the host atoms.

²Both direct and index notations are used in this paper for brevity and clarity as deemed necessary.

³Anisotropic interstitials, substitutional complexes and even vacancies are possible. In particular, one of the configurations yielded by quantum mechanical calculations of the relaxation around a vacancy in silicon is a tetragonal distortion of the four nearest-neighbors. In the equilibrium position after vacancy formation, all four atoms are at the same distance from the vacancy. However, the distances between the four atoms are not the same: The atoms form two pairs such that the distance separating the atoms in a pair is smaller than the distance separating each atom in one pair from the two in the other pair. This is the Jahn-Teller distortion, and in some instances has been calculated to have a lower formation energy than the isotropic distortion (Puska et al., 1998; Antonelli et al., 1998).

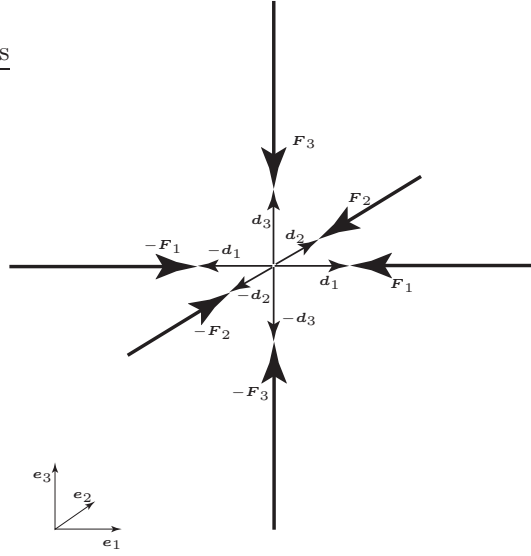


Figure 1: An arrangement of point forces leading to an isotropic dipole—specifically an isotropic vacancy or substitutional defect that is smaller than the host atoms.

Using (1), the force distribution due to the dipole is then written as

$$\mathbf{f}(\mathbf{x}) = -2 \sum_{i=1}^3 \mathbf{F}_i \otimes \mathbf{d}_i \nabla_{\mathbf{x}'} \delta(\mathbf{x} - \mathbf{x}')$$

or $\mathbf{f}(\mathbf{x}) = -\mathbf{D} \nabla_{\mathbf{x}'} \delta(\mathbf{x} - \mathbf{x}')$

where $\delta(\mathbf{x} - \mathbf{x}')$ is the three-dimensional Dirac-delta function that satisfies $\int h(\mathbf{x}) \delta(\mathbf{x} - \mathbf{x}') dV = h(\mathbf{x}')$ for a sufficiently smooth (C^∞) test function, $h(\mathbf{x})$. Since $\nabla_{\mathbf{x}'} \delta(\mathbf{x} - \mathbf{x}') = -\nabla_{\mathbf{x}} \delta(\mathbf{x} - \mathbf{x}')$, we finally have

$$\mathbf{f}(\mathbf{x}) = \mathbf{D} \nabla_{\mathbf{x}} \delta(\mathbf{x} - \mathbf{x}'). \quad (3)$$

The force distribution can be combined with the infinite space Green's function for anisotropic linear elasticity to obtain the displacement fields around the defect. The Green's function for elasticity, $\mathbf{G}(\mathbf{x} - \mathbf{x}')$, is a second-order tensor. For an anisotropic, linear medium it satisfies

$$\mathbb{C}_{ijkl} \frac{\partial^2 G_{km}}{\partial x_j \partial x_l} + \delta_{im} \delta(\mathbf{x} - \mathbf{x}') = 0, \quad (4)$$

where \mathbb{C}_{ijkl} is the fourth-order anisotropic elasticity tensor, G_{km} is the displacement at \mathbf{x} along \mathbf{e}_k due to a unit point force acting at \mathbf{x}' along \mathbf{e}_m , and δ_{im} is the Kronecker delta symbol. Barnett (1972) has applied the Fourier transform to derive analytic formulae for G_{ir} , its first and second spatial derivatives.

These formulae are summarized here:

$$G_{ir} = \frac{1}{4\pi^2|\mathbf{x} - \mathbf{x}'|} \int_0^\pi M_{ir}^*(\mathbf{z}(\Psi)) d\Psi, \quad (5)$$

$$\frac{\partial G_{ir}}{\partial x_s} = \frac{1}{4\pi^2|\mathbf{x} - \mathbf{x}'|^2} \int_0^\pi (-T_s M_{ir}^* + z_s H_{ir}) d\Psi, \quad (6)$$

$$\begin{aligned} \frac{\partial^2 G_{ir}}{\partial x_s \partial x_m} = \\ \frac{1}{4\pi^2|\mathbf{x} - \mathbf{x}'|^3} \int_0^\pi [2T_s T_m M_{ir}^* - 2(z_s T_m + z_m T_s) H_{ir} + z_s z_m A_{ir}] d\Psi. \end{aligned} \quad (7)$$

Letting \mathbf{k} denote the wave vector in Fourier space, $\mathbf{z} = \mathbf{k}/|\mathbf{k}|$ is a unit vector in Fourier space; $\mathbf{M}^* \mathbf{M} = \mathbf{1}$, where $M_{ir}(\mathbf{z}) = \mathbb{C}_{ijrs} z_j z_s$; $\mathbf{T} = (\mathbf{x} - \mathbf{x}')/|\mathbf{x} - \mathbf{x}'|$ is a unit vector in real space; Ψ is the polar angle in the plane $\mathbf{z} \cdot \mathbf{T} = 0$. Using these tensors and vectors \mathbf{H} and \mathbf{A} are defined as

$$\begin{aligned} H_{ir} &= \mathbb{C}_{jpnw} M_{ij}^* M_{nr}^* (z_p T_w + z_w T_p) \\ A_{ir} &= \mathbb{C}_{jpnw} [(z_p T_w + z_w T_p) (H_{ij} M_{nr}^* + M_{ij}^* H_{nr}) - 2M_{ij}^* M_{nr}^* T_p T_w]. \end{aligned}$$

2.1 The displacement and strain fields of a point defect

The displacement field of a point defect can be written using (3) and the Green's function:

$$\mathbf{u}^\infty(\mathbf{x}) = \int_{\mathbb{R}^3} \mathbf{G}(\mathbf{x} - \mathbf{x}') \mathbf{D} \nabla_{\mathbf{x}'} \delta(\mathbf{x}' - \mathbf{x}'') dV',$$

where the superscript on the left hand-side signifies the infinite space solution. Observe that the variable of integration is \mathbf{x}' . Reverting to indicial notation for clarity, and using a standard result on derivatives of distributions, this gives,

$$u_i^\infty(\mathbf{x}) = - \int_{\mathbb{R}^3} \left[\frac{\partial}{\partial x'_k} G_{ij}(\mathbf{x} - \mathbf{x}') \right] D_{jk} \delta(\mathbf{x}' - \mathbf{x}'') dV'.$$

Using $\partial G_{ij}(\mathbf{x} - \mathbf{x}')/\partial x'_k = -\partial G_{ij}(\mathbf{x} - \mathbf{x}')/\partial x_k$, and the definition of the Dirac-delta function we have

$$u_i^\infty(\mathbf{x}) = \frac{\partial G_{ij}(\mathbf{x} - \mathbf{x}'')}{\partial x_k} D_{jk}. \quad (8)$$

For an isotropic dipole, $D_{jk} = D\delta_{jk}$, this simplifies to

$$u_i^\infty(\mathbf{x}) = D \frac{\partial}{\partial x_j} G_{ij}(\mathbf{x} - \mathbf{x}''). \quad (9)$$

The strain field is written as

$$\varepsilon_{il}^\infty = \frac{1}{2} \left(\frac{\partial^2 G_{ij}}{\partial x_k \partial x_l} + \frac{\partial^2 G_{lj}}{\partial x_k \partial x_i} \right) D_{jk}, \quad (10)$$

which, for an isotropic dipole, simplifies to

$$\varepsilon_{il}^\infty = D \frac{1}{2} \left(\frac{\partial^2 G_{ij}}{\partial x_j \partial x_l} + \frac{\partial^2 G_{lj}}{\partial x_j \partial x_i} \right). \quad (11)$$

Evaluation of (8) and (10) involves the direct application of (6) and (7) respectively.

3 The formation volume tensor

3.1 The influence of boundaries

The formation volume tensor of a point defect can now be established using the center of contraction or expansion model. The results of Section 2.1 for infinite crystals are first extended to finite crystals in order to compare with the atomistic calculations to be described in Section 3.3. The development in this subsection was suggested to the authors by Barnett (2004) for the *scalar* formation volume, $\text{tr}[\mathbf{V}^f]$. The extension to the full tensor has not appeared before to the knowledge of the authors.

The formation volume tensor, V_{kl}^f , is the sum of tensorial volume changes due to relaxation of the crystal around the center of contraction or expansion, V_{kl}^r , and the addition of an atomic volume, $\frac{1}{3}\Omega\delta_{kl}$. The second term arises since the displaced atom's volume is added to the crystal. Note the assumption of isotropy associated with this step. We obtain an expression for V_{kl}^f below that, in addition to having other implications, demonstrates that V_{kl}^r , and therefore V_{kl}^f , are well-defined quantities.

For a defect in a finite crystal, B_{crys} , we define

$$V_{kl}^f \equiv \underbrace{\int_{B_{\text{crys}}} \varepsilon_{kl} dV}_{V_{kl}^r} + \frac{1}{3}\Omega\delta_{kl}, \quad (12)$$

where ε_{kl} is the strain field in the finite crystal due to the center of contraction or expansion with the appropriate value of the dipole. Using the stress-strain relation, this is

$$V_{kl}^f = \mathbb{S}_{kl ij} \int_{B_{\text{crys}}} \sigma_{ij} dV + \frac{1}{3}\Omega\delta_{kl} \quad (13)$$

where $\mathbb{S}_{kl ij}$ is the constant compliance tensor satisfying $\mathbb{S}_{kl ij} \mathbb{C}_{ij mn} = \mathbb{I}_{kl mn}$, the fourth-order symmetric identity tensor. Observe that

$$\int_{B_{\text{crys}}} \sigma_{ij} dV = \int_{B_{\text{crys}}} \left[\frac{\partial (x_i \sigma_{mj})}{\partial x_m} - x_i \frac{\partial \sigma_{mj}}{\partial x_m} \right] dV. \quad (14)$$

Using (3) the equilibrium equation for the center of contraction or expansion is written as

$$\frac{\partial \sigma_{jm}}{\partial x_m} + D_{jm} \frac{\partial \delta(\mathbf{x} - \mathbf{x}')}{\partial x_m} = 0. \quad (15)$$

Combining (14) and (15) and using the symmetry of $\boldsymbol{\sigma}$ we have,

$$\int_{B_{\text{crys}}} \sigma_{ij} dV = \int_{B_{\text{crys}}} \left[\frac{\partial (x_i \sigma_{mj})}{\partial x_m} + x_i D_{jm} \frac{\partial \delta(\mathbf{x} - \mathbf{x}')}{\partial x_m} \right] dV.$$

Using the standard result for spatial derivative of the Dirac-delta function, the symmetry of $\boldsymbol{\sigma}$, and the Divergence Theorem,

$$\int_{B_{\text{crys}}} \sigma_{ij} dV = \int_{S_{\text{crys}}} x_i \sigma_{jm} n_m dA - D_{jm} \delta_{im},$$

where S_{crys} is the surface of the crystal. Substituting this equation in (13) we have

$$V_{kl}^f = -\mathbb{S}_{klij} D_{ji} + \underbrace{\mathbb{S}_{klij} \int_{S_{\text{crys}}} x_i \sigma_{jm} n_m dA}_{V_{kl}^r} + \frac{1}{3} \Omega \delta_{kl}. \quad (16)$$

This result has three important, related, consequences: (i) The relaxation and formation volume tensors for a crystal with traction-free boundaries depend only on the strength of the center of contraction or expansion, represented here by the dipole D_{ji} , elasticity of the crystal, and the atomic volume (for the case of formation volume). In particular, neither the shape and size of the crystal nor the location of the center of contraction or expansion inside the crystal influence the outcome. (ii) The difference in V_{kl}^f between the case with traction-free boundary and one with arbitrary boundary conditions can be evaluated. For pure traction boundary conditions this is trivial. With displacement boundary conditions the elasticity problem must be solved first, possibly by numerical methods. (iii) Formation and relaxation volume tensors, unorthodox notions in continuum mechanics, can be defined in a precise fashion.

3.2 A thermodynamic basis for V^f

The center of contraction or expansion model for a point defect thus leads to a relation for V^f that can be evaluated if the stress field of the crystal is known. However, the thermodynamic basis of this quantity has not been clarified beyond the formal relation $V^f = -\partial \mathcal{G}^f / \partial \boldsymbol{\sigma}^{\text{ex}}$. In this subsection it is demonstrated that a result of Eshelby (1957), established for continuum inclusions, also holds in the center of contraction or expansion limit and provides such a thermodynamic basis.

We begin with the continuum result for the work of interaction between the traction, $\boldsymbol{\sigma}^{\text{ex}} \mathbf{n}$, applied at the boundary of a crystal, and the deformation

induced by a transforming inclusion in the crystal. As alluded to in Section 1, Eshelby showed that this work of interaction has the form

$$\mathcal{W}^{\text{ex}} = \int_{B_{\text{inc}}} \boldsymbol{\sigma}^{\text{ex}} : \boldsymbol{\varepsilon}^{\text{r}} dV \quad (17)$$

where B_{inc} is the region occupied by the inclusion before it undergoes the *stress-free* relaxation strain $\boldsymbol{\varepsilon}^{\text{r}}$ (Eshelby, 1957). This is the strain in the inclusion if its boundary, S_{inc} , is traction-free. If the inclusion is small enough that $\boldsymbol{\sigma}^{\text{ex}}$ is constant over B_{inc} , then following (12) and defining $\mathbf{V}_{\text{inc}}^{\text{r}} \equiv \int_{B_{\text{inc}}} \boldsymbol{\varepsilon}^{\text{r}} dV$ allows us to rewrite (17) as

$$\mathcal{W}^{\text{ex}} = \boldsymbol{\sigma}^{\text{ex}} : \mathbf{V}_{\text{inc}}^{\text{r}}. \quad (18)$$

A seemingly obvious step is to link $\mathbf{V}_{\text{inc}}^{\text{r}}$ and \mathbf{V}^{r} for the point defect. Then Eshelby's result would apply to the work of relaxation around a point defect, and the work of formation would be $\boldsymbol{\sigma}^{\text{ex}} : (\mathbf{V}^{\text{r}} + \frac{1}{3}\Omega\mathbf{1})$. Introducing this work term into the Gibbs free energy would lead to $\mathbf{V}^{\text{f}} = -\partial\mathcal{G}^{\text{f}}/\partial\boldsymbol{\sigma}^{\text{ex}}$. Such an approach has been adopted by Aziz et al. (1991). In our notation their expression is $\mathcal{W}^{\text{ex}} = \boldsymbol{\sigma}^{\text{ex}} : \boldsymbol{\varepsilon}^{\text{T}} \cdot \text{Vol}(B_{\text{inc}})$, where $\boldsymbol{\varepsilon}^{\text{T}}$ is the uniform transformation strain undergone by a “sub-system”, B_{inc} . However, there are technical difficulties in making such a direct association: (i) The boundary between the continuum inclusion and the solid in which it is embedded is well-defined, but it is not possible to precisely demarcate a lattice point defect in this manner. For example, Figure 2 shows a vacancy in a silicon crystal where the $\langle 100 \rangle$ direction is perpendicular to the plane of the figure (this is a visualization of one of our atomistic calculations). It is evident that no precise interface exists between the defect and the perfect lattice. Indeed, in the above expression used by Aziz and co-workers the extent of the “sub-system” is not made precise beyond a statement that it contains the atoms “involved in the fluctuation” of the transformation. The transformation strain is also not made precise. (ii) The arguments that Eshelby used in arriving at (17) require that the continuum assumption holds even in the neighborhood of the inclusion. The discreteness of the lattice clearly negates this assumption in the neighborhood of a point defect.

The center of contraction or expansion model of the point defect in continuum linear elasticity enables a circumvention of these difficulties: Consider a finite crystal with traction-free boundaries that is also stress-free in its interior. As before, B_{crys} is the domain of the crystal and its boundary is S_{crys} . Let an external traction, $\boldsymbol{\sigma}^{\text{ex}}\mathbf{n}$ be applied at S_{crys} . Also let $\boldsymbol{\varepsilon}^{\text{ex}}$ and \mathbf{u}^{ex} be the related strain and displacement fields in B_{crys} . Now let a point defect form in the interior of B_{crys} with corresponding dipole tensor \mathbf{D} . Let the stress, strain and displacement fields arising from this defect be $\boldsymbol{\sigma}^{\text{F}}$, $\boldsymbol{\varepsilon}^{\text{F}}$ and \mathbf{u}^{F} in the case that S_{crys} is traction-free. Also recall that according to the linear theory of elasticity the fields actually obtained now are $\boldsymbol{\sigma}^{\text{ex}} + \boldsymbol{\sigma}^{\text{F}}$, $\boldsymbol{\varepsilon}^{\text{ex}} + \boldsymbol{\varepsilon}^{\text{F}}$ and $\mathbf{u}^{\text{ex}} + \mathbf{u}^{\text{F}}$. The quantity of interest is the work done by the external stress on the crystal in the

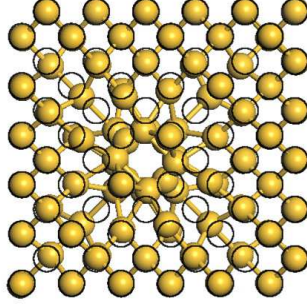


Figure 2: A vacancy in silicon viewed along the $\langle 100 \rangle$ direction. The open circles mark positions of atoms in the perfect crystal; i.e., before vacancy formation. Displacements have been scaled $10\times$ for clarity.

process of defect formation:

$$\mathcal{W}^{\text{ex}} = \int_{S_{\text{crys}}} u_i^{\text{F}} (\sigma_{ij}^{\text{ex}} n_j) dA.$$

Using the Divergence Theorem and integration by parts this is

$$\mathcal{W}^{\text{ex}} = \int_{B_{\text{crys}}} (u_i^{\text{F}} \sigma_{ij,j}^{\text{ex}} + \varepsilon_{ij}^{\text{F}} \sigma_{ij}^{\text{ex}}) dV,$$

where the symmetry of σ^{ex} has been used to restrict the displacement gradient to its symmetric part, the strain. Since σ^{ex} is divergence-free in B_{crys} the first term in the above integrand vanishes. The second term is rewritten using the stress-strain relations to give

$$\mathcal{W}^{\text{ex}} = \int_{B_{\text{crys}}} \sigma_{ij}^{\text{F}} \varepsilon_{ij}^{\text{ex}} dV.$$

Invoking the symmetry of σ^{F} and using integration by parts,

$$\mathcal{W}^{\text{ex}} = \int_{S_{\text{crys}}} u_i^{\text{ex}} \sigma_{ij}^{\text{F}} n_j dA - \int_{B_{\text{crys}}} u_i^{\text{ex}} \sigma_{ij,j}^{\text{F}} dV.$$

Since σ^{F} is obtained as the solution to the traction-free boundary case, the first term in this integrand vanishes. The second term is rewritten using $\sigma_{ij,j}^{\text{F}} + D_{ij} \delta_{,j}(\mathbf{x} - \mathbf{x}') = 0$, for a defect at $\mathbf{x} = \mathbf{x}'$, to give

$$\mathcal{W}^{\text{ex}} = \int_{B_{\text{crys}}} u_i^{\text{ex}} D_{ij} \frac{\partial}{\partial x_j} \delta(\mathbf{x} - \mathbf{x}') dV.$$

Using the standard result for derivative of the Dirac-delta function this gives

$$\mathcal{W}^{\text{ex}} = -u_{i,j}^{\text{ex}}(\mathbf{x}')D_{ij}.$$

For a symmetric dipole tensor (cf Section 2)

$$\mathcal{W}^{\text{ex}} = -\varepsilon_{ij}^{\text{ex}}(\mathbf{x}')D_{ij}.$$

From the stress-strain relations in the form $\varepsilon_{ij}^{\text{ex}} = \mathbb{S}_{ijkl}\sigma_{kl}^{\text{ex}}$ and the major and minor symmetries of \mathbb{S}_{ijkl} we have

$$\mathcal{W}^{\text{ex}} = \sigma_{kl}^{\text{ex}}(\mathbf{x}')(-\mathbb{S}_{klij}D_{ji}).$$

Finally, recalling (16) and noting that $\sigma_{jm}n_m$ in the boundary integral of that equation is now replaced by $\sigma_{jm}^{\text{F}}n_m = 0$ we have

$$\mathcal{W}^{\text{ex}} = \sigma_{kl}^{\text{ex}}V_{kl}^{\text{r}}. \quad (19)$$

On including the contribution of the displaced atom as in Section 3.1, this result can be extended to the work done in defect formation:

$$\mathcal{W}^{\text{ex}} = \sigma_{kl}^{\text{ex}}\left(V_{kl}^{\text{r}} + \frac{1}{3}\Omega\delta_{kl}\right) = \sigma_{kl}^{\text{ex}}V_{kl}^{\text{f}}. \quad (20)$$

The use of (20) for \mathcal{W}^{ex} in \mathcal{G}^{f} lends rigor to the thermodynamic definition $\mathbf{V}^{\text{f}} \equiv -\partial\mathcal{G}^{\text{f}}/\partial\boldsymbol{\sigma}^{\text{ex}}$ (Section 1). By extension through $\mathbf{V}^{\text{r}} = \mathbf{V}^{\text{f}} - \frac{1}{3}\Omega\mathbf{1}$ this development also provides a thermodynamic basis for \mathbf{V}^{r} . Thus the center of contraction or expansion model makes the notion of formation and relaxation volume tensors precise, and also provides a thermodynamic basis for these quantities.

Remark 1: Nowick and Heller (1963) have defined a volume tensor analogous to \mathbf{V}^{r} . Their expression is $v\lambda_{ij}$, where v is the atomic volume and λ_{ij} is what they call an “elastic dipole tensor”. The volume tensor $v\lambda_{ij}$ is conjugate to the external stress via the interaction energy. However, λ_{ij} is “equal to the average strain per mole fraction of defects all aligned in a particular orientation”. This definition is therefore considerably different from our treatment. To our knowledge neither this definition of a volume tensor nor that of Aziz et al. (1991) has been rigorously *derived* in a kinematic or thermodynamic sense. Our search of the literature on point defects has not uncovered either a kinematic definition of \mathbf{V}^{r} as in Section 3.1 or a thermodynamic basis for it as in Section 3.2.

3.3 Atomistic calculations for the formation volume and dipole

The solution for any elastic field around the center of contraction or expansion depends on the dipole strength, \mathbf{D} , which must be known to fully specify the elasticity problem. Thus, the formation volume, \mathbf{V}^{f} , cannot be obtained from elasticity alone. The dipole, \mathbf{D} , and hence \mathbf{V}^{f} , must be obtained from

atomistic calculations using empirical interatomic potentials, tight binding or *ab initio* methods. A comparison between such atomistic calculations and a simple continuum result allows a determination of \mathbf{D} in closed-form as shown in Section 3.3.1. With the value of \mathbf{D} thus known, continuum elasticity can be used for a variety of calculations involving the elastic fields around the point defect. In Section 3.4 we show that the elasticity results of Section 3.1 also provide important information regarding the validity of atomistic calculations for $\text{tr}[\mathbf{V}^f]$. The results of Section 4.3 similarly demonstrate the importance of interactions between the vacancy, elastic fields and boundary loading mechanism in determining the strain energy of formation, \mathcal{U}^f .

We have undertaken atomistic calculations of vacancy formation using the Stillinger-Weber interatomic potential (Stillinger and Weber, 1985). Although this empirical potential is a rough approximation of silicon, particularly at the defect, it is suitable for the purpose of checking consistency between continuum elastic and atomistic predictions for \mathbf{V}^f and \mathcal{U}^f in the far-field.

The Stillinger-Weber potential consists of two- and three-body terms governing the interactions of N atoms:

$$\Phi(1, \dots, N) = \sum_{i < j}^N v_2(r_{ij}) + \sum_{i < j < k}^N v_3(\mathbf{r}_i, \mathbf{r}_j, \mathbf{r}_k) \quad (21)$$

$$v_2(r_{ij}) = e f_2\left(\frac{r_{ij}}{\xi}\right) \quad (22)$$

$$v_3(\mathbf{r}_i, \mathbf{r}_j, \mathbf{r}_k) = e f_3\left(\frac{\mathbf{r}_i}{\xi}, \frac{\mathbf{r}_j}{\xi}, \frac{\mathbf{r}_k}{\xi}\right) \quad (23)$$

where energy and length units e and ξ are chosen to give f_2 a minimum value of -1 if its argument is $2^{1/6}$. The two-body function, f_2 , depends only on the distance $r_{ij} = |\mathbf{r}_i - \mathbf{r}_j|$ between a pair of atoms with position vectors \mathbf{r}_i and \mathbf{r}_j and has a cut-off at $r = a$ without discontinuities in any derivatives with respect to r :

$$f_2(r) = \begin{cases} A(Br^{-p} - r^{-q}) \exp(\frac{1}{r-a}) & : \text{if } r < a, \\ 0 & : \text{if } r \geq a \end{cases} \quad (24)$$

The three-body function, f_3 , depends on the scalar distances between the three atoms and also on the angle subtended at the vertices of the triangle formed by the three atoms. In the following relations θ_{jik} is the angle subtended at vertex i between atoms with position vectors \mathbf{r}_j and \mathbf{r}_k :

$$f_3\left(\frac{\mathbf{r}_i}{\xi}, \frac{\mathbf{r}_j}{\xi}, \frac{\mathbf{r}_k}{\xi}\right) = h\left(\frac{r_{ij}}{\xi}, \frac{r_{ik}}{\xi}, \theta_{jik}\right) + h\left(\frac{r_{ji}}{\xi}, \frac{r_{jk}}{\xi}, \theta_{ijk}\right) + h\left(\frac{r_{ki}}{\xi}, \frac{r_{kj}}{\xi}, \theta_{ikj}\right) \quad (25)$$

$$h(r_1, r_2, \theta) = \begin{cases} \lambda \exp\left(\frac{\gamma}{r_1-a} + \frac{\gamma}{r_2-a}\right) \left(\cos \theta + \frac{1}{3}\right)^2 & : r_1 \text{ and } r_2 < a \\ 0 & : r_1 \text{ or } r_2 \geq a. \end{cases} \quad (26)$$

The equilibrium bond angle in the tetrahedral structure of silicon satisfies $\cos \theta = -1/3$. The energetic contribution of any bond angle distortions are thus represented by the trigonometric term in (26). The lattice spacing and bond energy of silicon at 0 K are obtained with $\xi = 0.20951$ nm and $e = 2.346$ eV.

The optimized set of parameters for this function is:

$$\begin{aligned} A &= 7.049556277, & B &= 0.6022245584 \\ p &= 4, \quad q = 0, & a &= 1.80 \\ \lambda &= 21.0, & \gamma &= 1.20. \end{aligned}$$

Energy minimization calculations were performed using the conjugate gradient method for system sizes ranging from 64 to 64,000 atoms. The smallest of these systems is comparable to moderate-sized *ab initio* calculations. (We are unaware of point defect calculations with *ab initio* methods having more than 512 atoms.) The computational cells were cubic in shape. Separate calculations were run with with periodic and free boundary conditions respectively. In each case the perfect crystal was equilibrated from randomized initial conditions for the atoms. Subsequently, the central atom was removed to model a vacancy and the system was allowed to equilibrate again. The simulations in periodic cells were run at zero average normal traction over each face by including a Lagrange multiplier that is energy-conjugate to the cell size. At each iteration of the algorithm the total energy was minimized and the cell size was varied to obtain zero average normal traction on each of the six faces.

The energy minimization calculations yielded a mean formation volume over the different system sizes of $\text{tr}[\mathbf{V}^f] = -13.8 \text{ \AA}^3$ in the minimum energy configuration. This is to be compared with the atomic volume of silicon which is $\Omega = 20 \text{ \AA}^3$, implying a relaxation volume of $\text{tr}[\mathbf{V}^r] = -33.8 \text{ \AA}^3$ according to (16).

Remark 2: The value of $\text{tr}[\mathbf{V}^f] = -13.8 \text{ \AA}^3$ suggests a rather strong relaxation in silicon, but is typical for the Stillinger-Weber model, which has previously been reported to result in large relaxations of the vacancy's nearest-neighbor atoms (Balamani et al., 1992). While the quantitative result is not expected to be physically accurate, the methodology established in this paper is of greater importance.

3.3.1 Tensorial form of \mathbf{V}^r

The atomistic calculations also yield the tensorial form of \mathbf{V}^r . The definition

$$V_{ij}^r = \int_{B_{\text{crys}}} \varepsilon_{ij} dV$$

can be rewritten as

$$V_{ij}^r = \int_{B_{\text{crys}}} \frac{1}{2} (u_{i,j} + u_{j,i}) dV$$

where \mathbf{u} now is the displacement field of relaxation around the defect obtained from the atomistic calculation. Gauss' Theorem then gives

$$V_{ij}^r = \int_{S_{\text{crys}}} \frac{1}{2} (u_i n_j + u_j n_i) dA. \quad (27)$$

With either periodic or traction-free boundary conditions, since the normal, \mathbf{n} , is fixed for a given surface of the computational cell, it follows that the integral in (27) reduces to the symmetric dyadic product of the areal average of each displacement component, $\int \mathbf{u} dA$, and \mathbf{n} . The symmetric distribution of the components u_j on a face with non-zero normal component n_i , for $j \neq i$ ensures that \mathbf{V}^r is a diagonal tensor. Symmetry with respect to the three basis vectors, $\{\mathbf{e}_1, \mathbf{e}_2, \mathbf{e}_3\}$, then ensures isotropy of \mathbf{V}^r . These numerical results were borne out in the atomistic calculations to a reasonable degree of accuracy. The tensors \mathbf{V}^r , obtained for 512 and 64,000 atom calculations using this formula, are recorded in Appendix A. The averages and standard deviations over a number of samples are reported.

Equation (27) can be applied to any atomistic calculation to determine V_{ij}^r . In combination with (16) it uniquely determines the defect dipole tensor, D_{ij} . If the atomistic calculation does not involve traction-free boundary conditions, the discrete analogue of the surface integral in (16) can be determined very easily from the atomistic results by an obvious generalization of the procedure used below in Section 3.4. This establishes the thermodynamically-correct relation for V_{ij}^f or V_{ij}^r . The defect dipole tensor can then be calculated in closed form using (16) and (27).

3.4 Boundary conditions and defect symmetry in determining $\text{tr}[\mathbf{V}^r]$

In this section we evaluate the influence of the integral in (16) on the value obtained for the scalar relaxation volume, $\text{tr}[\mathbf{V}^r]$. We consider the cubic computational cells used in our atomistic calculations. The cell faces were aligned with the cubic crystal directions. We emphasize that the results of this subsection hold where the theory of linear elasticity remains valid. One may therefore expect that they will hold in the far-field of the point defect.

The contribution of the surface integral in (16) needs to be evaluated on any one face only since the contributions from the remaining faces are equal by symmetry. Consider the $[100]$ face, denoted by S_1 with $\mathbf{x} = \langle l, x_2, x_3 \rangle^T$, where l is the half-length of the computational cell and $-l \leq x_2, x_3 \leq l$. The unit outward normal to this face is $\mathbf{n}_1 = \langle 1, 0, 0 \rangle^T$. The components of the traction vector $\mathbf{t}^P = \boldsymbol{\sigma}^P \mathbf{n}_1$, for zero average normal stress, satisfy the following relations for an isotropic defect:

$$\int_{S_1} t_1^P dA = 0, \quad t_2^P = 0, \quad t_3^P = 0 \text{ on } S_1, \quad (28)$$

The integral condition on t_1^P follows from the zero average normal stress condition. (Hereafter, the phrase “periodic boundary conditions” will imply the zero average normal traction condition also, unless explicitly stated otherwise.) The pointwise conditions on the shear components t_2^P and t_3^P follow since the shear stress components σ_{21} and σ_{31} are zero on S_1 , which in turn follows from symmetry across the periodic boundary and isotropy of the defect. Therefore, the cubic anisotropy of silicon makes the trace of the boundary integral in (16) vanish when evaluated on S_1 :

$$\frac{1}{\mathbb{C}_{1111} + 2\mathbb{C}_{1122}} \int_{x_2=-l}^l \int_{x_3=-l}^l (t_1^P l + t_2^P x_2 + t_3^P x_3) dA = 0 \quad (29)$$

by Equation (28). Therefore, according to linear elasticity, the periodic boundary conditions result in the same scalar relaxation volume as the traction-free boundary, provided the defect is isotropic and located at the center of the periodic cell. From (16) we have

$$\text{tr}[\mathbf{V}^f] = -\frac{1}{\mathbb{C}_{1111} + 2\mathbb{C}_{1122}} \text{tr}[\mathbf{D}] + \Omega,$$

for silicon with cubic anisotropy and an isotropic point defect. Therefore, according to linear elasticity, the calculation of $\text{tr}[\mathbf{V}^f]$ is also unaffected by the choice of periodic or traction-free boundary conditions.

With $\text{tr}[\mathbf{V}^r] = -33.8 \text{ \AA}^3$ from the atomistic calculation, $\mathbb{C}_{1111} = 1.616 \times 10^{11}$ Pa and $\mathbb{C}_{1122} = 0.816 \times 10^{11}$ Pa for Stillinger-Weber silicon, (Balamane et al., 1992) this gives a dipole strength $\text{tr}[\mathbf{D}] = 36.594 \times 10^{-19}$ N-m for the isotropic vacancy in the Stillinger-Weber model.

Figure 3 presents atomistic data for $\text{tr}[\mathbf{V}^f] = \text{tr}[\mathbf{V}^r] + \Omega$ as a function of number of atoms used in the calculations. Several calculations were performed for each choice of system size (number of atoms). These simulations were started from randomized initial positions of atoms. Each data point represents the formation volume of the calculation with the lowest energy for the given number of atoms. The relative independence of $\text{tr}[\mathbf{V}^f]$ obtained by using periodic boundary conditions bears out the result in (29). The results from atomistic simulations with traction-free boundaries are also shown. The relatively slow convergence of these results with system size arises from the fact that the atoms on the surface are not identical in bonding coordination to the bulk atoms. This also leads to the departure from the elasticity result that $\text{tr}[\mathbf{V}^f]$ is independent of the nature of the boundary condition (periodic/free). This discrepancy becomes negligible for systems having 64,000 atoms.⁴ The implication is that independence from type of boundary condition is obtained only in the larger systems where elastic effects dominate.

⁴However, for systems much bigger than 64,000 atoms, the sheer number of atoms introduces many more spurious minima in the energy minimization calculations. The conjugate gradient algorithm tends to get “trapped” in these spurious minima, leading to larger errors in the relaxation volumes that are obtained.

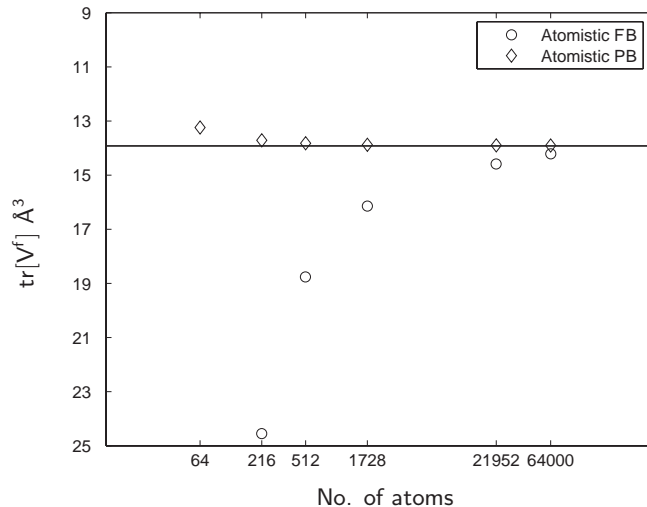


Figure 3: Comparison of formation volume calculated by atomic relaxation for traction-free boundary conditions (Atomistic FB) and periodic boundary conditions (Atomistic PB).

Remark 3: The result of an atomistic calculation for $\text{tr}[\mathbf{V}^f]$ has been shown to be independent of the shape and location of the boundary relative to isotropic point defects centered in a computational cell with periodic boundary conditions. It is therefore independent of the size of the crystal and depends only on \mathbf{D} , the elasticity of the crystal, and the atomic volume. This type of boundary condition is therefore well-suited for volume change calculations of isotropic defects.

4 The strain energy of formation

The observed dependence of \mathbf{V}^f on boundary conditions in (16) motivates a similar examination of the dependence of the strain energy of formation. In the continuum setting it proves convenient to begin such an analysis with an infinite crystal and subsequently subject it to cutting and welding operations in the manner of Eshelby (1957, 1961) in order to address finite crystals. Let B_{crys} now denote a simply-connected finite subset of the infinite crystal enclosing the center of contraction or expansion. Let \mathbf{n} denote the unit outward normal to B_{crys} . Let the strain energy in the region B_{crys} be $\mathcal{U}_{\infty_V}^f$, and the strain energy of the infinite crystal be \mathcal{U}_{∞}^f . These energies are related as follows:

$$\mathcal{U}_{\infty}^f = \mathcal{U}_{\infty_V}^f + \int_{\mathbb{R}^3 \setminus B_{\text{crys}}} \frac{1}{2} \sigma_{ij}^{\infty} \varepsilon_{ij}^{\infty} dV.$$

Applying the Divergence Theorem to the integral, and noting that $\sigma_{ij,j}^\infty = 0$ exterior to B_{crys} , leads to

$$\mathcal{W}_\infty^f = \mathcal{W}_{\infty_V}^f - \int_{S_{\text{crys}}} \frac{1}{2} \sigma_{ij}^\infty n_j u_i^\infty dV. \quad (30)$$

We will not pursue an explicit expression for \mathcal{W}_∞^f or $\mathcal{W}_{\infty_V}^f$. Instead we will relate them to the strain energy of a finite crystal with boundary S_{crys} .

4.1 Finite crystal with traction-free boundaries

Now consider turning B_{crys} into a finite crystal with traction-free boundaries. This can be achieved by holding the traction fixed at $\sigma_{ij}^\infty n_j$ on S_{crys} , cutting along this surface, and then applying a traction $\sigma_{ij}^F n_j = -\sigma_{ij}^\infty n_j$ to S_{crys} , where σ_{ij}^F is the image stress field so produced in B_{crys} . Let the corresponding displacement field be denoted by u_i^F , and its strain field by $\varepsilon_{ij}^F = \mathbb{C}_{ijkl}^{-1} \sigma_{kl}^F$. The relation between the strain energy in this configuration, $\mathcal{W}_{F_V}^f$, and $\mathcal{W}_{\infty_V}^f$ is

$$\mathcal{W}_{\infty_V}^f = \mathcal{W}_{F_V}^f + \int_{B_{\text{crys}}} \frac{1}{2} (-\sigma_{ij}^F) (-\varepsilon_{ij}^F) dV,$$

where we have used the fact that the stress field $-\sigma_{ij}^F$ applied to the traction-free crystal results in a strain field $-\varepsilon_{ij}^F$ in B_{crys} , returning it to the configuration with energy $\mathcal{W}_{\infty_V}^f$. Furthermore, we have used the result that there is no interaction energy between an external traction, $-\sigma_{ij}^F n_j$, and the internal stress, $\sigma_{ij}^F + \sigma_{ij}^\infty$, since the internal stress state is traction free $[(\sigma_{ij}^F + \sigma_{ij}^\infty) n_j = 0$ by construction] at the boundary, S_{crys} .

Using integration by parts, the Divergence Theorem, and the fact that $\sigma_{ij,j}^F = 0$ this is reduced to

$$\mathcal{W}_{\infty_V}^f = \mathcal{W}_{F_V}^f + \int_{S_{\text{crys}}} \frac{1}{2} \sigma_{ij}^F n_j u_i^F dA. \quad (31)$$

From (30) and (31) combined with the result $\sigma_{ij}^F n_j = -\sigma_{ij}^\infty n_j$ at S_{crys} , we have

$$\mathcal{W}_\infty^f = \mathcal{W}_{F_V}^f - \int_{S_{\text{crys}}} \frac{1}{2} \sigma_{ij}^\infty n_j (u_i^F + u_i^\infty) dA. \quad (32)$$

4.2 Finite crystal of cubic shape and periodic boundaries

Consider a cube-shaped domain, B_{crys} . Periodic boundary conditions imposed on the displacement at constant cell volume imply that the total displacement vanishes on S_{crys} . This state is obtained by subjecting the final configuration with traction-free boundaries to the additional boundary displacement $u_i^P = -u_i^\infty - u_i^F$ at S_{crys} . Let ε_{ij}^P be the corresponding strain field over B_{crys} , and

$\sigma_{ij}^P = \mathbb{C}_{ijkl}\varepsilon_{kl}^P$ be the stress field in B_{crys} . Now, the strain energy of the crystal is

$$\mathcal{U}_{P_V}^f = \mathcal{U}_{F_V}^f + \int_{B_{\text{crys}}} \frac{1}{2} \sigma_{ij}^P \varepsilon_{ij}^P dV,$$

where the absence of interaction energy between σ_{ij}^P and the internal stress with $(\sigma_{ij}^F + \sigma_{ij}^\infty)n_j = 0$ on S_{crys} has been used. Using integration by parts, the Divergence Theorem, and the fact that $\sigma_{ij,j}^P = 0$ we have

$$\mathcal{U}_{P_V}^f = \mathcal{U}_{F_V}^f + \int_{S_{\text{crys}}} \frac{1}{2} \sigma_{ij}^P n_j u_i^P dA. \quad (33)$$

The implications of (30–33) for the thermodynamics of point defect formation are elaborated in Sections 4.3 and 5 below.

Remark 4: We have used the symbol \mathcal{U}^f for the strain energies of formation, since, for the purely mechanical processes considered in this paper, the change in internal energy, \mathcal{U}^f , is the strain energy when we only consider the crystal away from the defect. An additional contribution to the formation energy arises from the change in bonding at the defect, which is, of course, not represented in elasticity.

4.3 Numerical evaluation of strain energies of formation

The strain energy of formation with traction-free boundaries on a cubic computational cell was numerically-evaluated as follows: The stress at the boundaries of the cubic computational cell embedded in an infinite crystal was obtained from (10) and $\sigma_{ij}^\infty = \mathbb{C}_{ijkl}\varepsilon_{kl}^\infty$. The resulting force distribution on a surface, S_α , of the computational cell was considered, where the surface normal was denoted by $\mathbf{n}_\alpha = \frac{\alpha}{|\alpha|} \mathbf{e}_{|\alpha|}$, $\alpha = \{\pm 1, \pm 2, \pm 3\}$. The subscript $(\bullet)_{|\alpha|}$ denotes $(\bullet)_1$, $(\bullet)_2$ or $(\bullet)_3$. The force distribution was represented by point forces $T_{iM}(\mathbf{x}_M) = \sigma_{ij}^\infty(\mathbf{x}_M)n_{\alpha_j}A_M$, with A_M , $M = 1, \dots, N_{\text{nd}}^2$ being the area associated with N_{nd}^2 points, \mathbf{x}_M , on each surface of the computational cell. These points subsequently defined the surface nodes of a finite element discretization of the computational cell with N_{nd}^3 nodes. The finite element mesh had equal-sized, trilinear, cubic elements. For such a mesh, A_M equals the area of each face of the cubic elements for a point that does not lie on an edge or vertex of the computational cell; A_M equals half the area of each face of the cubic elements for a point on an edge; and A_M equals quarter the area of each face of the cubic elements for a point on a vertex.

Image forces were applied on the nodes of S_α by reversing the above-computed nodal forces so that, when superposed on the tractions $\sigma_{ij}^\infty n_{\alpha_j}$, the resulting field at the boundary nodes was traction-free. The displacement field u_i^F due to these nodal image forces on the boundary was obtained as the finite element

displacement solution, and the integral in (32) was calculated as

$$\mathcal{U}_\infty^f - \mathcal{U}_{FV}^f = - \int_{S_{\text{cryst}}} \frac{1}{2} \sigma_{ij}^\infty n_j (u_i^F + u_i^\infty) dA = -\frac{1}{2} \sum_{\substack{\alpha=-3 \\ \alpha \neq 0}}^3 \sum_{n=1}^{N_{\text{nd}}} T_{i_n} (u_{i_n}^F + u_{i_n}^\infty). \quad (34)$$

This is the difference in energies between the infinite crystal and the traction-free boundary case. The calculations were carried out for $\text{tr}[\mathbf{D}] = 36.594 \times 10^{-19}$ N-m.

The difference between strain energies of the periodic boundary and free boundary cases, $\mathcal{U}_{PV}^f - \mathcal{U}_{FV}^f$ is given by the integral in (33). Recall that in the atomistic calculations with periodic boundary conditions, the computational cell was also relaxed to have zero average normal traction, and pointwise zero shear tractions on the surfaces. In the finite element calculations this was achieved by applying the following traction field over the surface S_α :

$$\bar{t}_i^R = \begin{cases} \frac{1}{\text{Area}(S_\alpha)} \int_{S_\alpha} (-\sigma_{ij}^P n_{\alpha_j}) dA & , \text{ if } i = |\alpha|, \\ -\sigma_{ij}^P n_{\alpha_j} & , \text{ if } i \neq |\alpha|. \end{cases} \quad (35)$$

Note that while \bar{t}_i^R is constant over the surface S_α for $i = |\alpha|$, it varies over S_α for $i \neq |\alpha|$.

Let the displacement field u_i^R result from application of traction \bar{t}_i^R defined as in (35) over each surface, S_α . Since \bar{t}_i^R is constant over S_α for $i = |\alpha|$, and the shear components do not give rise to normal strains in a cubic material, it follows that u_i^R is constant over S_α for $i = |\alpha|$.

In order to extend (33) to the periodic boundary condition calculation with zero average normal traction, the integral in that equation was replaced by

$$\sum_{\substack{\alpha=-3 \\ \alpha \neq 0}}^3 \int_{S_\alpha} (\bar{t}_{\alpha_i}^R + \sigma_{ij}^P n_{\alpha_j}) (-u_i^\infty - u_i^F + u_i^R) dA,$$

where $-u_i^\infty - u_i^F = u_i^P$. From (35) and $u_i^R = \text{const}$ on S_α for $i = |\alpha|$, this integral is

$$\mathcal{U}_{PV}^f - \mathcal{U}_{FV}^f = \sum_{\substack{\alpha=-3 \\ \alpha \neq 0}}^3 \int_{S_\alpha} (\bar{t}_i^R + \sigma_{ij}^P n_{\alpha_j}) (-u_i^\infty - u_i^F) dA. \quad (36)$$

The finite element displacement solution obtained for $-u_i^F$ was added to the infinite crystal displacement field $-u_i^\infty$. This field, $-u_i^\infty - u_i^F$, evaluated on the boundaries, S_α , was then reapplied as a displacement boundary condition to the finite element mesh to obtain the surface traction field $\sigma_{ij}^P n_{\alpha_j}$. Then (35) and (36) gave the required energy difference.

Figure 4 is a comparison of the energy differences $\mathcal{U}_\infty^f - \mathcal{U}_{FV}^f$ and $\mathcal{U}_\infty^f - \mathcal{U}_{PV}^f$ obtained with the atomistic and elasticity calculations. The actual value of

\mathcal{U}_∞^f , has not been obtained directly from elasticity. However, the integrals in (34) and (36) both are $\mathcal{O}(r^{-3})$, where $2r$ is the characteristic linear dimension of the computational cell. Therefore, \mathcal{U}_{FV}^f and \mathcal{U}_{PV}^f converge to \mathcal{U}_∞^f as $r \rightarrow \infty$. Since $r^{-3} \propto N^{-1}$, where N is the number of atoms in the system, this convergence is confirmed in Figure 4. Analysis of (32) and (33), or of (34) and (36) indicates that \mathcal{U}_{FV}^f and \mathcal{U}_{PV}^f converge to \mathcal{U}_∞^f from below. Figure 4 confirms this prediction, since the energy differences $\mathcal{U}_\infty^f - \mathcal{U}_{(\bullet)}^f$ are all positive. The trends are replicated by the atomistic calculations, in which \mathcal{U}_{FV}^f and \mathcal{U}_{PV}^f are directly calculated. The asymptotic value to which \mathcal{U}_{FV}^f and \mathcal{U}_{PV}^f converge in the atomistic calculations has been used as \mathcal{U}_∞^f .

The discrepancy between linear elasticity and atomistic calculations for the smaller cells (e.g. 512 atoms) in Figure 4 is most probably due to the highly nonlinear deformations around the vacancy that dominate at these small scales. The 512-atom computational cell is made up of $4 \times 4 \times 4$ Si unit cells. The boundary is only 10.86 Å away from the vacancy. At such small scales linear elasticity provides a poor estimate of the strain energy of the highly distorted lattice around the vacancy.

The difference between the energies of the traction-free and periodic boundaries with the atomistic calculations in Figure 4 most probably is a manifestation of an interaction energy in the near field of the defect: The periodic boundary configuration effectively applies a boundary traction to the traction-free configuration, as explained above. This external stress field interacts with the internal stress of the traction-free boundary configuration. Such an interaction energy, however, vanishes according to the theory of linear elasticity. This result has been employed in Sections 4.1 and 4.2, and is possibly responsible for the very small differences observed between \mathcal{U}_{FV}^f and \mathcal{U}_{PV}^f using linear elasticity. For the smaller cells, the strong nonlinear effect possibly invalidates this result of linear elasticity causing the discrepancy in $\mathcal{U}_{PV}^f - \mathcal{U}_{FV}^f$ between the atomistic and linear elasticity calculations. The trends, however, are the same: The free and periodic boundary cases converge from below to the infinite crystal result. The periodic boundary case is higher in strain energy due to the imposed constraint that preserves the flat shape of the cubic cell's boundaries. This difference, while small, exists in the elasticity calculations also as seen in Table 1.

5 Conclusions

The central conclusions from this work are the following:

1. Equation (16) implies that the formation volume of a point defect is a well-defined quantity. It is to be measured on a crystal whose surfaces are traction-free. Defined in this manner, it depends only on the strength of the defect, the elasticity of the material and the atomic volume. It is independent of the crystal's shape and size, and of the location of the defect within the crystal.

Table 1: Comparison of strain energy of vacancy formation in a cubic cell with periodic and traction-free boundaries—elasticity results. For comparison, the atomistic calculations converge to $\mathcal{U}_\infty^f = 2.8237$ eV. Note that the cell sizes, expressed as number of Si atoms that make up a crystal of the same size, do not correspond exactly to the cell sizes actually used in the atomistic calculations.

Cell size in number of atoms	$\mathcal{U}_{PV}^f - \mathcal{U}_{FV}^f$ (μeV)
512	45.791
4096	5.759
13824	1.714
46656	0.510
110592	0.215

2. On the basis of Item 1 above, Equation (16) provides an exact quantitative measure of the appropriateness of any class of boundary conditions used on an atomistic calculation to extract formation volumes of point defects.
3. The derivation ending in Equations (19) and (20) demonstrates that Eshelby’s calculation (17) on the work done by external stress on a transforming inclusion has an analogue for point defects. This is an exact result. It provides a rigorous thermodynamic basis for the concepts of formation and relaxation volume tensors that goes beyond formal definitions of the type $\mathbf{V}^f = -\partial\mathcal{G}^f/\partial\boldsymbol{\sigma}^{\text{ex}}$.
4. The combination of (27) and (16) provides a closed-form expression for the defect dipole tensor that can be determined from any atomistic calculation.
5. Equations (30–33) quantify the influence of traction-free and periodic boundary conditions on the strain energy of formation of point defects according to continuum linear elasticity. In each case, the corresponding boundary integrals can be calculated. Significant discrepancies are observed between the continuum elastic and atomistic results for the smallest system sizes (512 atoms) because the highly nonlinear lattice distortion around the defect permeates the entire computational cell when the latter is composed of a small number of atoms. Linear elasticity is not an accurate theory for such nonlinear distortions. Additionally, for atomistic systems of this size, there appears to be an interaction energy between an externally-applied boundary traction and an internal stress field with vanishing traction at the boundary. According to linear elasticity this interaction energy vanishes exactly. This could lead to the much smaller difference in strain energies of formation between the traction-free and periodic boundary cases obtained via linear elasticity. Indeed, this suggests that (31–33) are not accurate for systems smaller than roughly 4000 atoms.
6. The difference between strain energies of vacancy formation obtained with traction-free boundaries and periodic boundaries (that are traction free

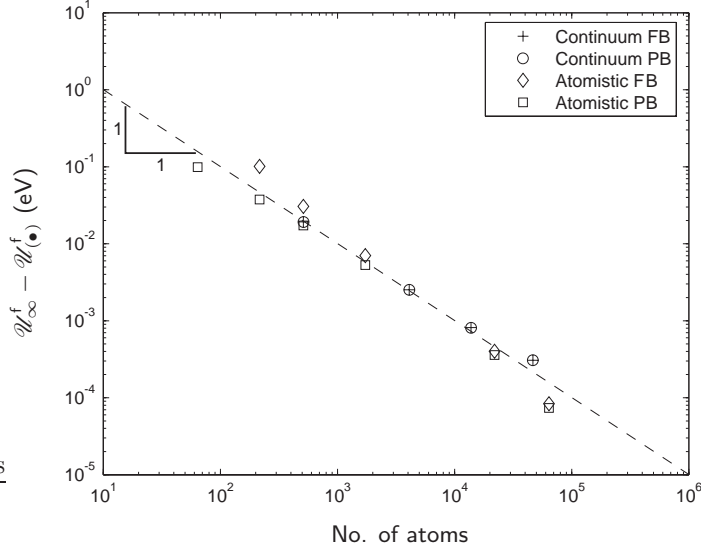


Figure 4: Comparison of strain energies of formation calculated by atomic relaxation and elasticity for periodic (PB) and traction-free (FB) boundary conditions.

on average) vanishes with increasing cell size. Linear elasticity predicts that the scalar vacancy formation volumes, however, are identical for an isotropic defect that is centered in the computational cell. Yet, the atomistic results show significant differences for the scalar formation volume for the two types of boundary conditions (Figure 3) at smaller cells. This discrepancy can be attributed to the larger influence of boundary atoms' coordination numbers for small cells, and it diminishes for the larger calculations. We expect that this discrepancy will be enhanced, due to elasticity effects, for the much larger class of anisotropic point defects: vacancies with the Jahn-Teller distortion and most interstitial configurations, as well as for defects not located at the center of the periodic cell.

A Relaxation volume tensors from atomistic calculations

Representative relaxation volume tensors obtained from the energy minimization calculations on systems with varying numbers of atoms, and with traction-free or periodic boundary conditions are reported below. For the sake of brevity values are reported for only the 512- and 64,000-atom systems. Averages and standard deviations (SD) were calculated by running several calculations with starting positions of atoms varying randomly from the equilibrium positions in a

perfect crystal. The larger standard deviations for larger systems are associated with the spurious minima discussed in Footnote 4.

Traction-free boundary conditions with 512 atoms:

$$\mathbf{V}_{\text{av}}^{\text{r}} = \begin{bmatrix} -13.676 & 0.683 & 0.695 \\ 0.683 & -13.669 & 0.678 \\ 0.695 & 0.678 & -13.674 \end{bmatrix} \text{ \AA}^3, \quad \text{SD} = \begin{bmatrix} 0.192 & 0.030 & 0.031 \\ 0.030 & 0.172 & 0.027 \\ 0.031 & 0.027 & 0.151 \end{bmatrix} \text{ \AA}^3.$$

Periodic (traction-free on average) boundary conditions with 512 atoms:

$$\mathbf{V}_{\text{av}}^{\text{r}} = \begin{bmatrix} -12.009 & 0.706 & 0.706 \\ 0.706 & -12.009 & 0.706 \\ 0.706 & 0.706 & -12.009 \end{bmatrix} \text{ \AA}^3, \quad \text{SD} = \begin{bmatrix} 0.001 & 0.002 & 0.002 \\ 0.002 & 0.001 & 0.001 \\ 0.002 & 0.001 & 0.001 \end{bmatrix} \text{ \AA}^3.$$

Traction-free boundary conditions with 64,000 atoms:

$$\mathbf{V}_{\text{av}}^{\text{r}} = \begin{bmatrix} -11.625 & -0.022 & -0.021 \\ -0.022 & -11.484 & -0.029 \\ -0.021 & -0.029 & -11.421 \end{bmatrix} \text{ \AA}^3, \quad \text{SD} = \begin{bmatrix} 0.535 & 0.178 & 0.185 \\ 0.178 & 0.308 & 0.138 \\ 0.185 & 0.138 & 0.339 \end{bmatrix} \text{ \AA}^3.$$

Periodic (traction-free on average) boundary conditions with 64,000 atoms:

$$\mathbf{V}_{\text{av}}^{\text{r}} = \begin{bmatrix} -11.571 & -0.147 & -0.130 \\ -0.147 & -11.217 & -0.054 \\ -0.130 & -0.054 & -11.136 \end{bmatrix} \text{ \AA}^3, \quad \text{SD} = \begin{bmatrix} 0.653 & 0.115 & 0.057 \\ 0.115 & 0.473 & 0.142 \\ 0.057 & 0.142 & 0.363 \end{bmatrix} \text{ \AA}^3.$$

References

- Antonelli, A., Chadi, D. J., Kaxiras, E., 1998. Vacancy in silicon revisited: Structure and pressure effects. *Phys. Rev. Lett.* 81, 2088.
- Aziz, M. J., 1997. Thermodynamics of diffusion under pressure and stress: Relation to point defect mechanisms. *Appl. Phys. Lett* 70, 2810.
- Aziz, M. J., Sabin, P. C., G-Lu, 1991. The activation strain tensor: Nonhydrostatic stress effects on crystal-growth kinetics. *Phys. Rev. B* 44 (18), 9812.
- Balamane, H., Haliocioglu, T., Tiller, W. A., 1992. Comparative study of silicon empirical interatomic potentials. *Phys. Rev. B* 46, 2250.
- Barnett, D. M., 1972. The precise evaluation of derivatives of anisotropic elastic Green's functions. *Phys. Stat. Sol. B* 59, 741.
- Barnett, D. M., 2004. Private communication.

- Daw, M. S., Windl, W., Carlson, N. N., Laudon, M., Masquelier, M. P., 2001. Effect of stress on dopant and defect diffusion in Si: A general treatment. *Phys. Rev. B* 64, 045205.
- Eshelby, J. D., 1957. The determination of the elastic field of an ellipsoidal inclusion and related problems. *Proc. Roy. Soc. Lond. Ser. A* 241 (1226), 376.
- Eshelby, J. D., 1961. Elastic inclusions and inhomogeneities. In: Hill, R., Sneddon, J. (Eds.), *Progress in Solid Mechanics*. North Holland Publishing Co., p. 89.
- Nowick, A. S., Heller, W. R., 1963. Anelasticity and stress-induced ordering of point defects in crystals. *Adv. Phys.* 12, 251.
- Puska, M. J., Pöykkö, S., Pesola, M., Nieminen, R. M., 1998. Convergence of supercell calculations for point defects in semiconductors: Vacancy in silicon. *Phys. Rev. B* 58, 1318.
- Stillinger, F. H., Weber, T. A., 1985. Computer simulation of order in condensed phases of silicon. *Phys. Rev. B* 31, 5262.
- Zhao, Y., Aziz, M. J., Gossman, H. J., Mitha, S., Schiferl, D., 1999b. Activation volume for antimony diffusion in silicon and implications for strained films. *Appl. Phys. Lett.* 75, 941.
- Zhao, Y., Aziz, M. J., Gossman, H. J., Mitha, S., Schiferl, D., 1999a. Activation volume for boron diffusion in silicon and implications for strained films. *Appl. Phys. Lett.* 74, 31.